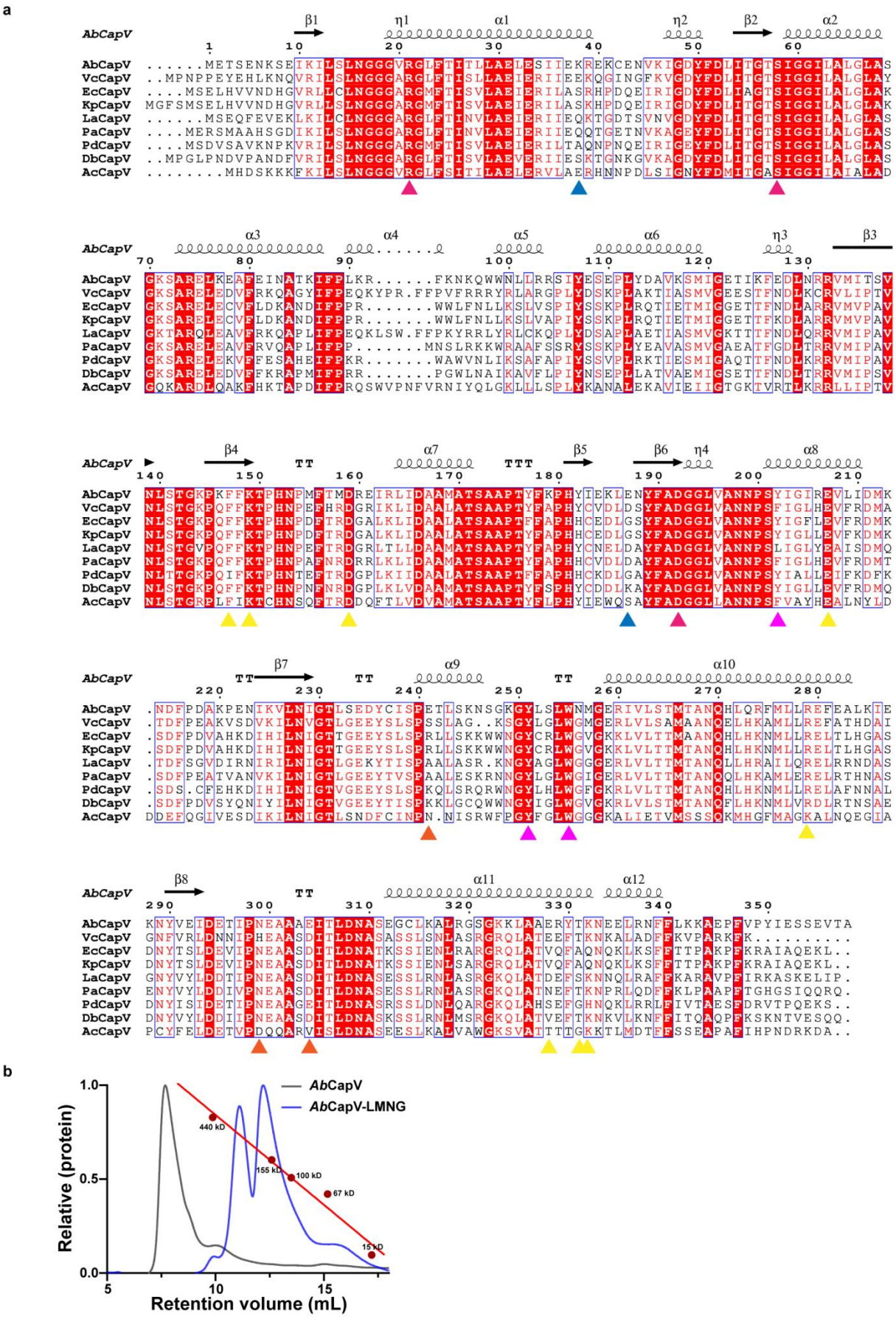

1 **Extended Data Fig. 1 CapV Proteins Are Phospholipases Activated by**

3’3’-cGAMP.

a, Alignment of divergent CapV homologs annotated with the determined secondary structure of *Ab*CapV. Different colored triangles mark distinct active sites: red indicates phospholipid binding and cleavage sites, yellow marks cGAMP binding sites, blue represents the AC interaction interface, orange marks the BC interaction interface, and pink highlights the AB interaction interface. **b,** SEC demonstrating the effect of LMNG on the aggregation state of protein purification. The addition of detergent changed the protein into homodimer and homotetramer. The standard curve is represented in red.

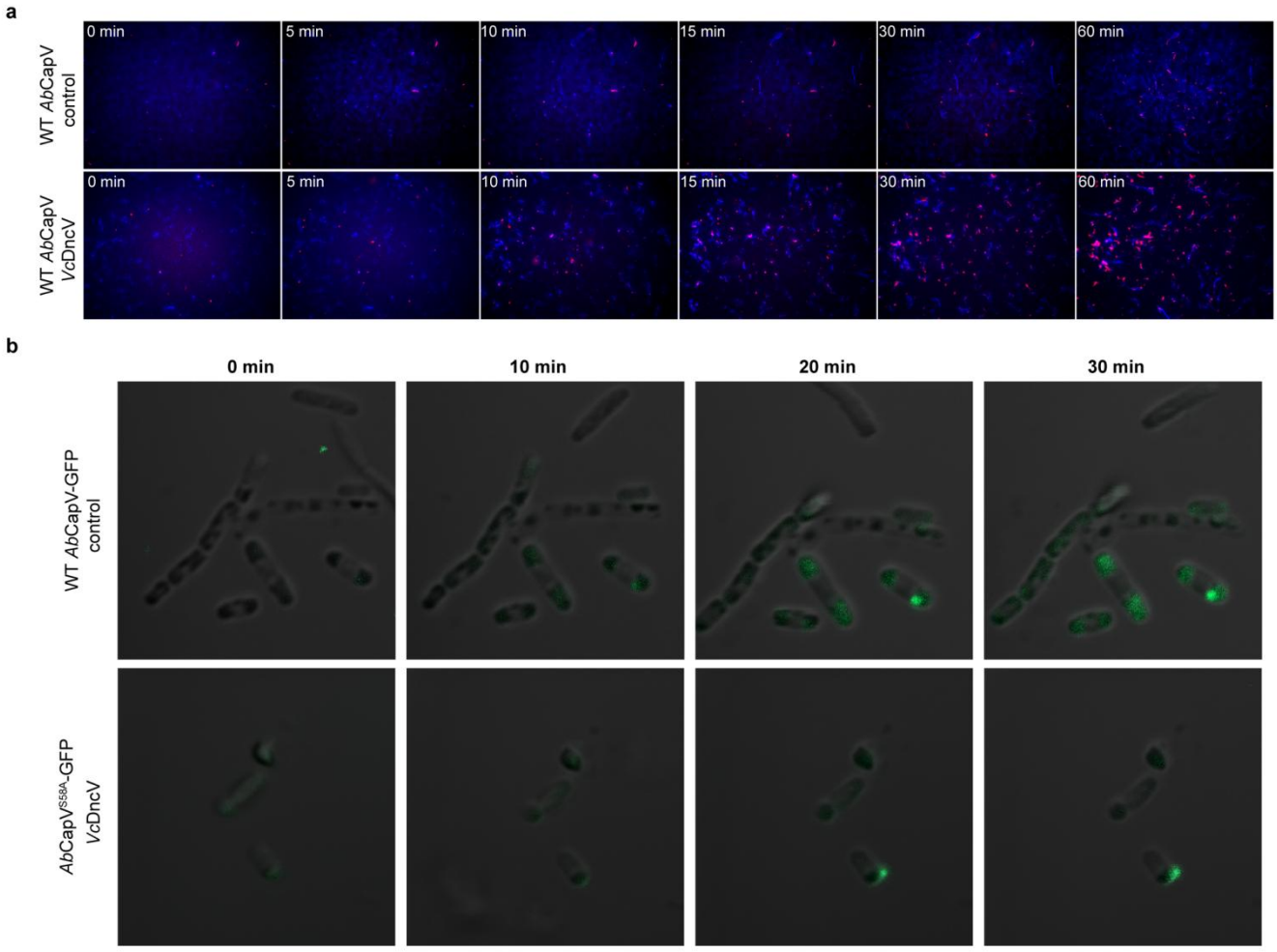

Extended Data Fig. 2 CapV activation causes membrane disruption of one pole and cell death.

a, Time-lapse fluorescence microscopy of E. coli expressing WT *Ab*CapV and *Vc*DncV or an *Ab*CapV control. DAPI staining and PI staining were used to evaluate the cell states. Strong DAPI-staining dots represent bacteriophage particles. **b,** Time-lapse Confocal microscopy of E. coli expressing *Ab*CapV^{S58A}-GFP and *Vc*DncV or an *Ab*CapV^{S58A}-GFP control.

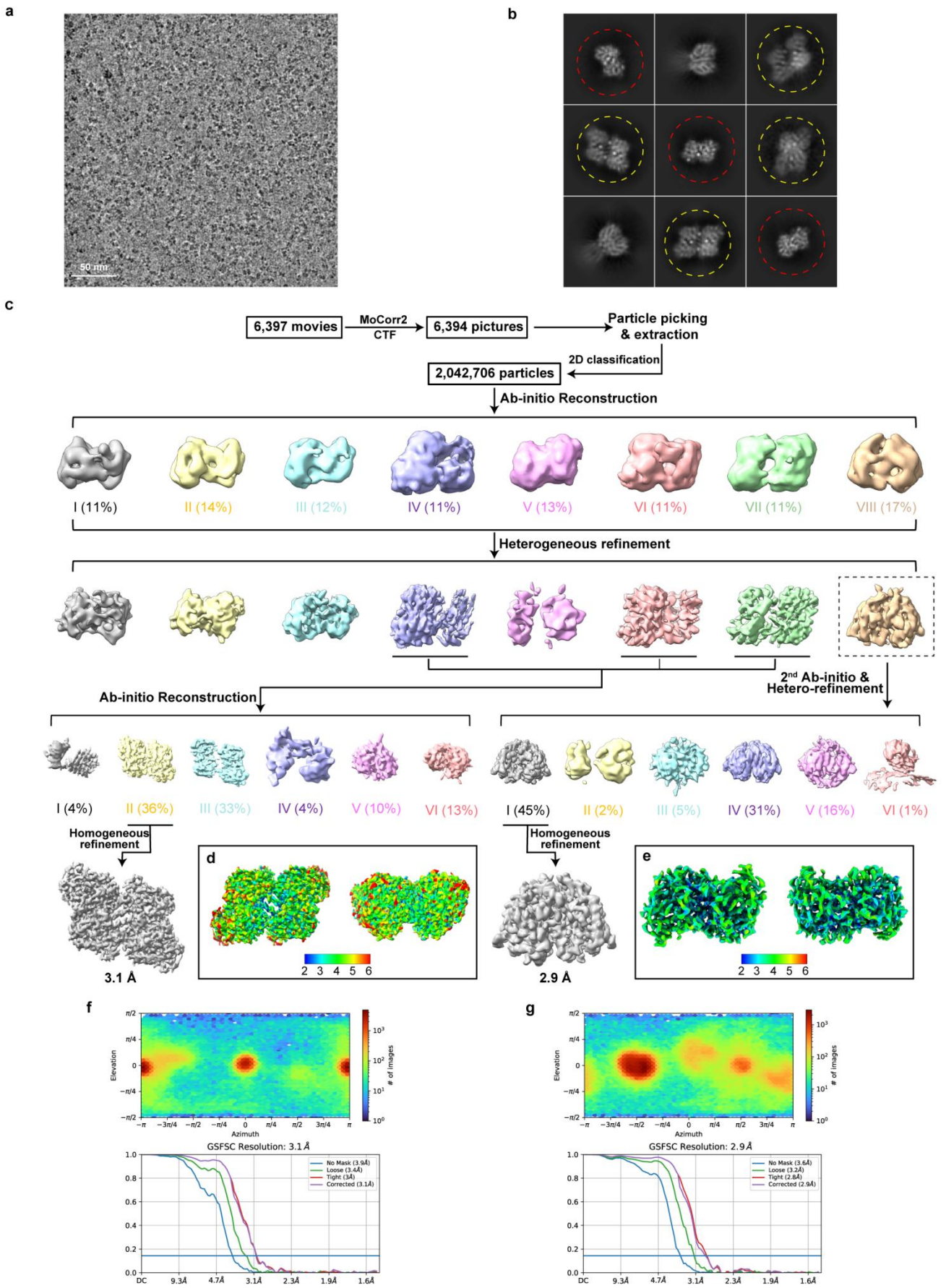
a
50 nm
b
c
6,397 movies
MoCorr2
CTF
6,394 pictures
Particle picking
& extraction
2D classification
2,042,706 particles
Ab-initio Reconstruction
I (11%)
II (14%)
III (12%)
IV (11%)
V (13%)
VI (11%)
VII (11%)
VIII (17%)
Heterogeneous refinement
Ab-initio Reconstruction
2nd Ab-initio &
Hetero-refinement
I (4%)
II (36%)
III (33%)
IV (4%)
V (10%)
VI (13%)
I (45%)
II (2%)
III (5%)
IV (31%)
V (16%)
VI (1%)
Homogeneous
refinement
Homogeneous
refinement
d
e
2 3 4 5 6
2 3 4 5 6
3.1 Å
2.9 Å
f
g
Elevation
Azimuth
# of images
GSFSC Resolution: 3.1 Å
GSFSC Resolution: 2.9 Å
No Mask (3.9Å)
Loose (3.4Å)
Tight (3Å)
Corrected (3.1Å)
No Mask (3.6Å)
Loose (3.2Å)
Tight (2.8Å)
Corrected (2.9Å)
DC
9.3Å
4.7Å
3.1Å
2.3Å
1.9Å
1.6Å

Extended Data Fig. 3 Cryo-EM data processing for *Ab*CapV apo state and intermediate state.

a, Section of a representative electron micrograph of *Ab*CapV apo state and intermediate state. **b,** Cryo-EM class averages of *Ab*CapV. Particle classification and quantification for each condition demonstrates that CapV has two oligomeric states. **c,** Flow chart of cryo-EM data analysis of *Ab*CapV. Two homo-oligomers (apo state and intermediate state) were obtained. Reconstructions of *Ab*CapV tetramer **(d)** and dimer **(e)** were coloured by local resolution. The viewing direction distribution plot and the 'gold-standar' Fourier shell correlation (FSC) curves of *Ab*CapV tetramer **(f)** and dimer **(g)** were presented.

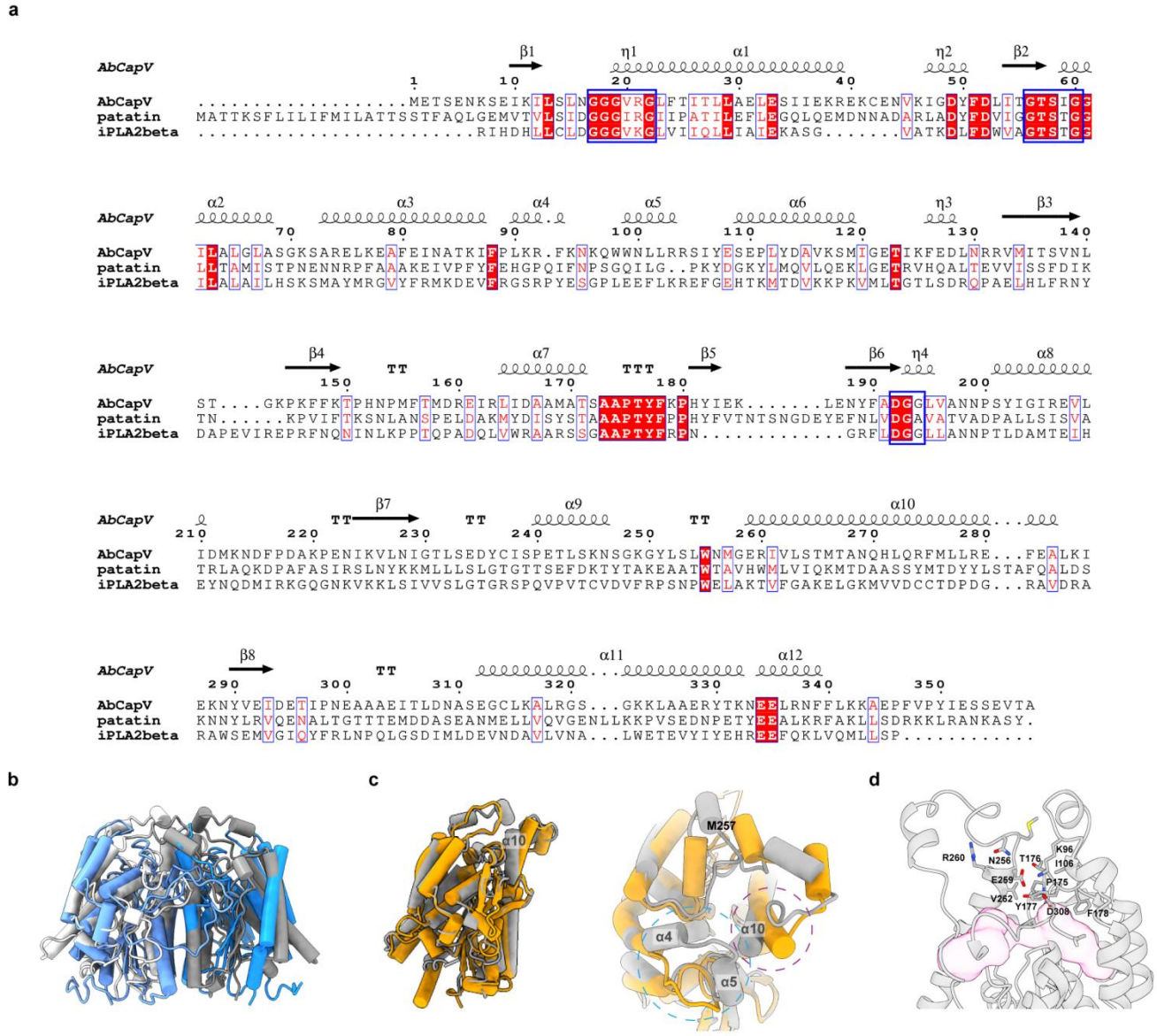

Extended Data Fig. 4 Alignment of *Ab*CapV and different patatin-like phospholipase A2.

a, Alignment of *Ab*CapV and different phospholipase A2 from plants (patatin-17) and mammals (iPLA$_2$β) annotated with the determined secondary structure of *Ab*CapV. The conserved motifs of the PNPLA domain were framed in blue. **b,** Comparison of CapV dimer and the CAT domain of iPLA$_2$β. The interaction between the two CAT domains in the iPLA$_2$β dimer is similar to that of CapV dimer. RMSD between 119 pruned atom pairs is 1.107 angstroms; (across all 288 pairs: 6.719) **c,** Comparison of CapV protomer and patatin-17. The monomer structure of Patatin-17 is highly similar to protomer of CapV (left). RMSD between 179 pruned atom pairs is 1.070 angstroms; (across all 312 pairs: 4.428). The phospholipid binding pocket of CapV and that of patatin-17 was enlarged (right). The main differences were circled with different color. **d,** Close-up views of the conserved phospholipid binding pocket of *Ab*CapV. The

volume of pocket was displayed with red density, and the side chains of the amino acids that block the channel have been displayed.

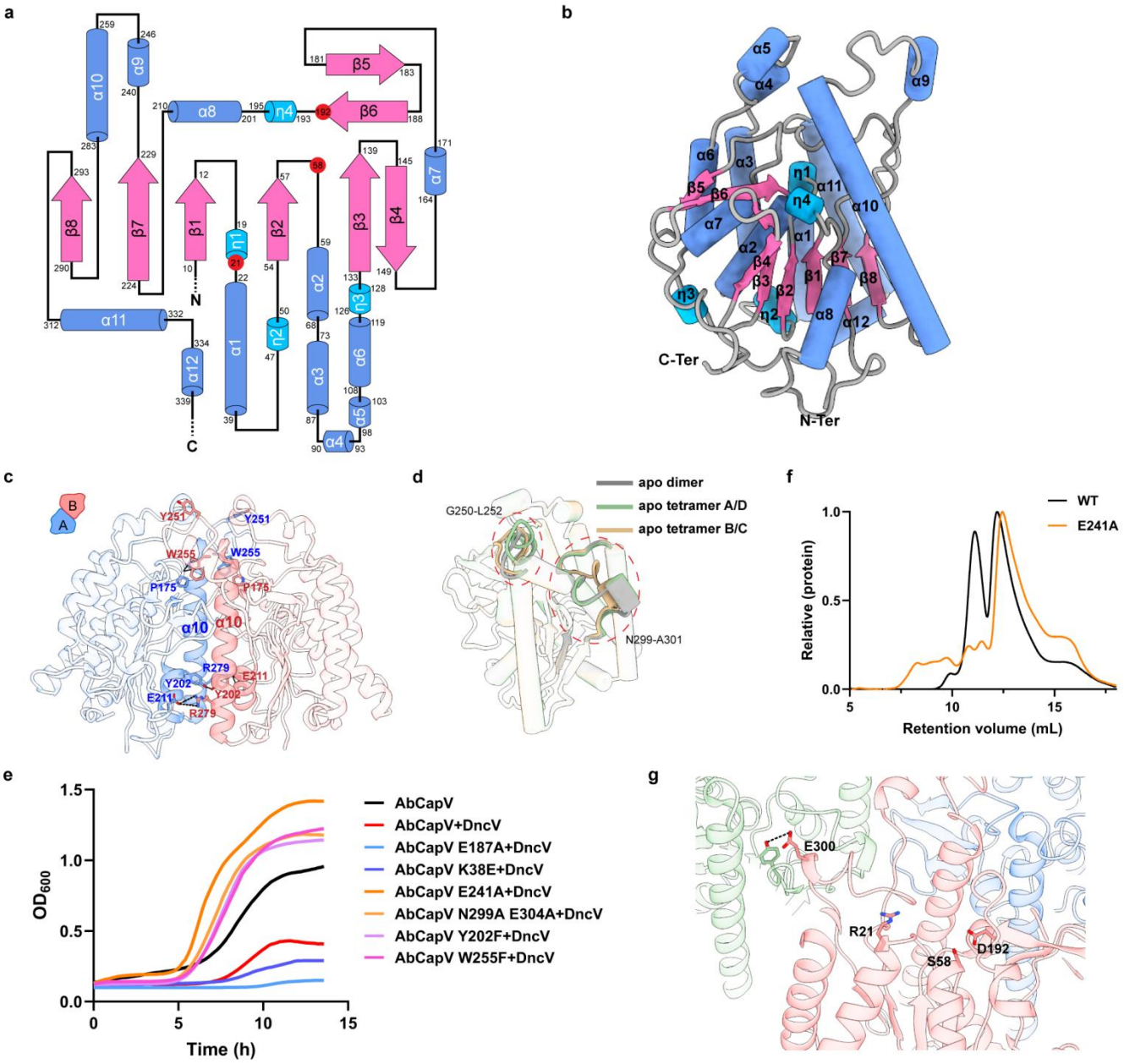

Extended Data Fig. 5 *Ab*CapV exists as dimer and tetramer.

a, The topology diagram of *Ab*CapV. Helices are shown as cylinders, and β sheets are shown as arrows. Three key active sites for phospholipid binding and hydrolysis are marked with red circles. **b,** The protomer structure from dimer labeled the secondary structure. **c,** Close-up views of *Ab*CapV apo dimer interface including major interaction residues, and the hydrogen bond is depicted as a black dashed line. **d,** Superposition of subunits of apo dimer and apo tetramer *Ab*CapV. The global changes have been highlighted. **e,** Growth curves of E. coli expressing *Vc*DncV and *Ab*CapV wt or interface mutants. The data are representative of more than three independent biological replicates each with three technical replicates. **f,** SEC demonstrating the effect of interface BC mutation E241A on aggregation state of apo protein. **g,** Expanded view of phospholipid-binding and cleavaging residues in apo tetramer.

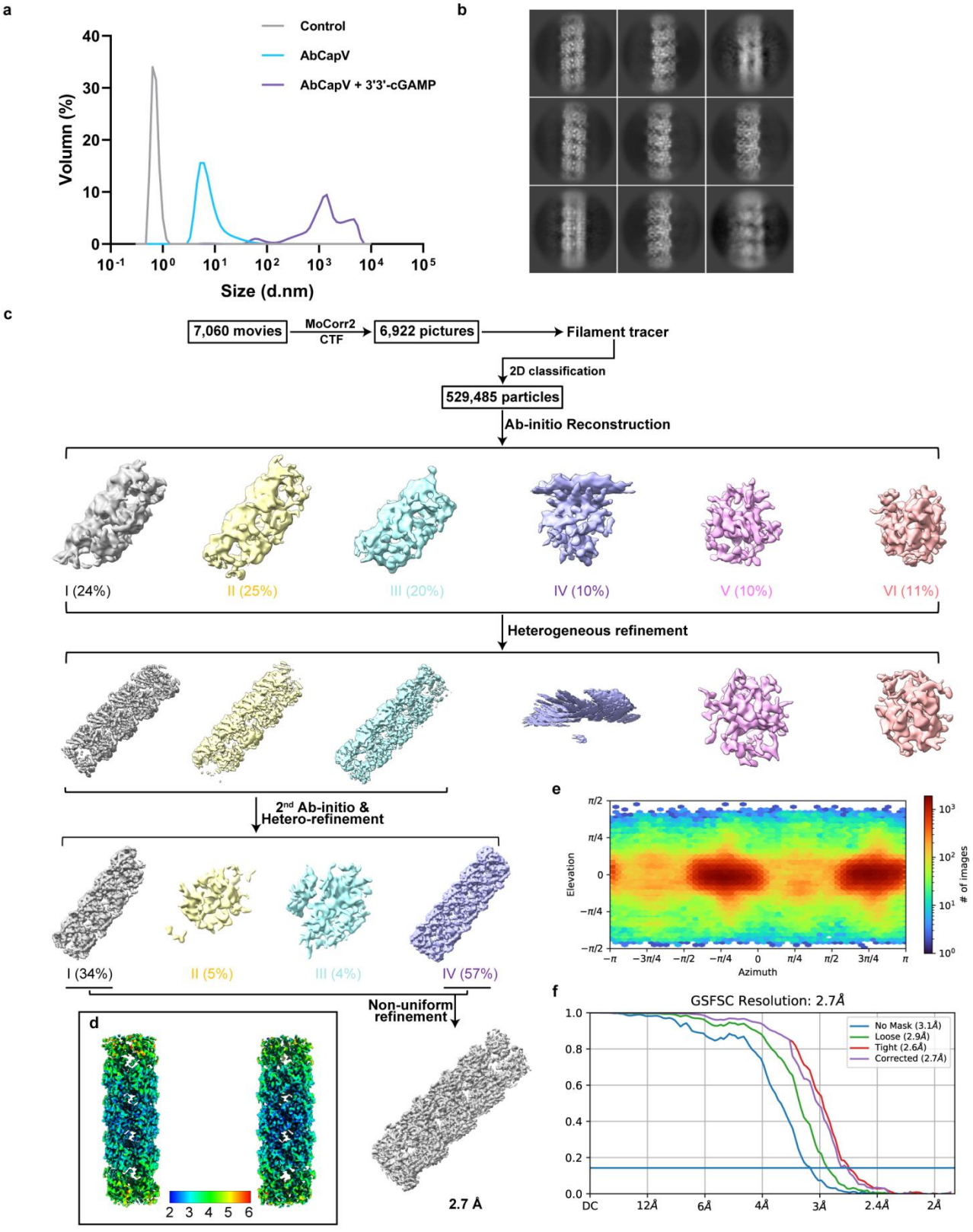

58 **Extended Data Fig. 6 Cryo-EM data processing for *Ab*CapV filament bound to**
59 **3'3'-cGAMP.**
60 **a,** Volume particle size distributions of purified *Ab*CapV in the presence of cGAMP
61 or other cyclic dinucleotides. **b,** Cryo-EM class averages of *Ab*CapV bound to

3’3’-cGAMP. CapV filaments occurs in the presence of activating 3’3’-cGAMP. **c,** Flow chart of cryo-EM data analysis of *Ab*CapV filaments. Two homo-oligomers were obtained. Reconstructions of *Ab*CapV filaments **(d)** was colored by local resolution. The viewing direction distribution plot **(e)** and the ‘gold-standard’ Fourier shell correlation (FSC) curves **(f)** of *Ab*CapV filaments were presented.

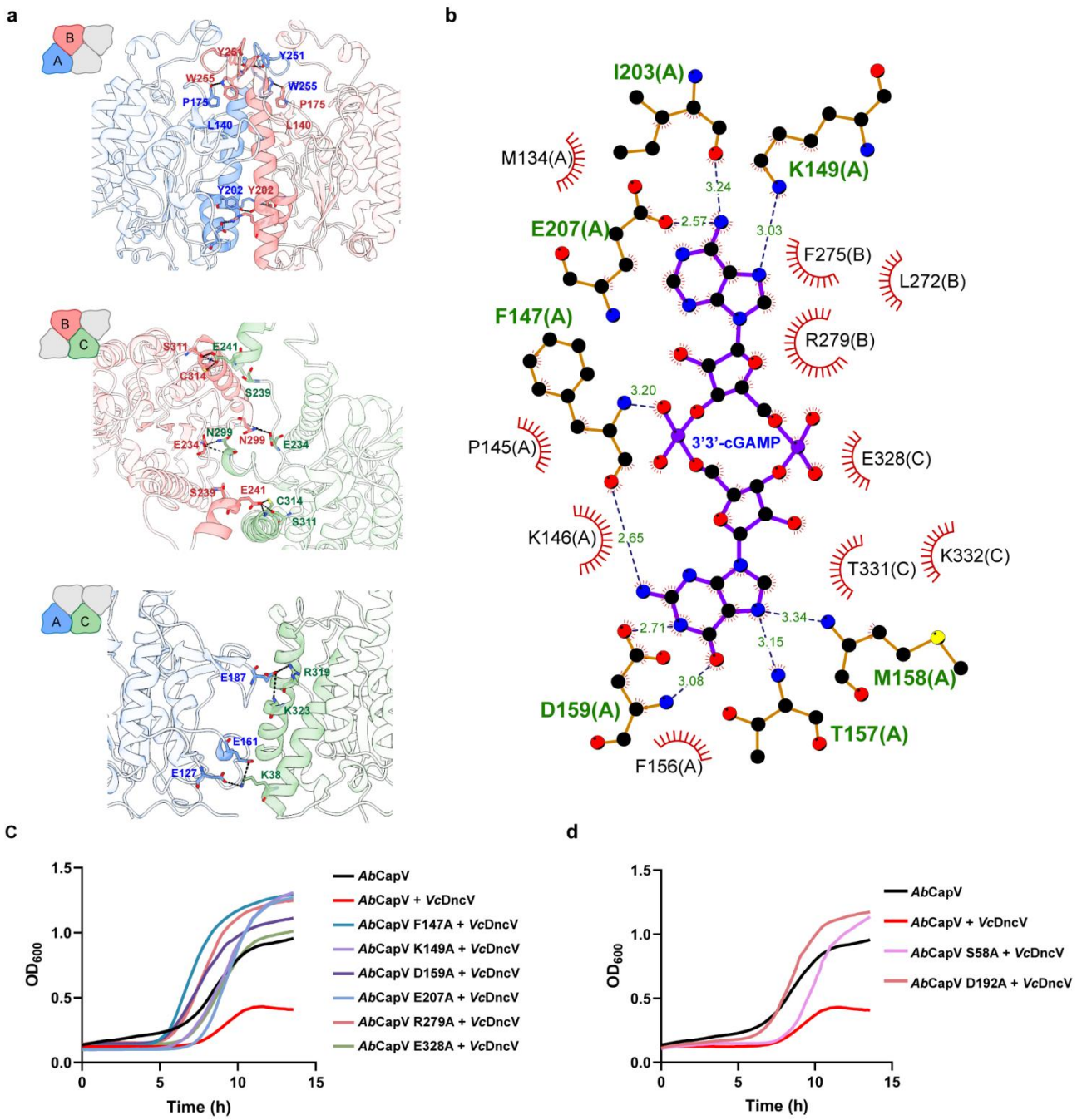

Extended Data Fig. 7 CapV is activated by 3'3'-cGAMP to form filament and cleave phospholipids.

a, Close-up views of *Ab*CapV filament interfaces including major interaction residues. Left, interface between protomer A and B. Middle, interface between protomer A and C. Right, interface between protomer B and C. Those residues in the interaction interface were labeled. **b,** LigPlot+ of the interactions between *Ab*CapV and 3'3'-cGAMP. Numbers in colour specify inter-atom distances in Å. Hydrogen atoms are omitted. **c,** Growth curves of E. coli expressing *Vc*DncV and *Ab*CapV wt or cGAMP binding site mutants. The data are representative of more than three independent biological replicates each with three technical replicates. **d,** Growth curves of E. coli expressing *Vc*DncV and *Ab*CapV wt or phospholipid binding site

mutants. The data show means of three independent replicates. The data are representative of more than three independent biological replicates each with three technical replicates.

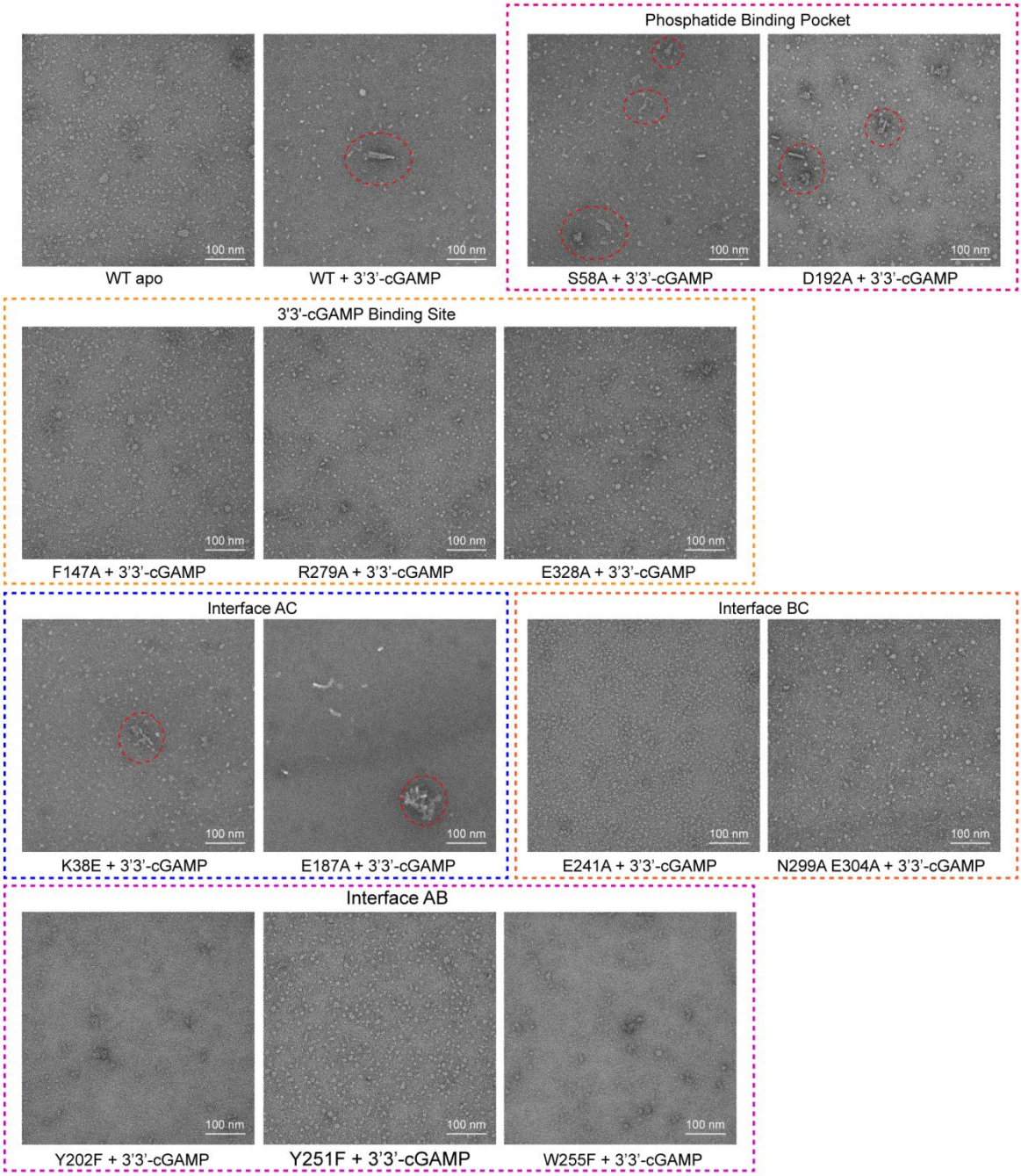

Extended Data Fig. 8 3'3'-cGAMP mediated phospholipid cleavage activity is driven by *Ab*CapV oligomerization.

Negative-stain micrograph images for wild type *Ab*CapV and mutants in the presence of 3'3'-cGAMP (right) or not (left). The aggregation of proteins were circled in red. Each image is representative of n = 6 micrograph images.

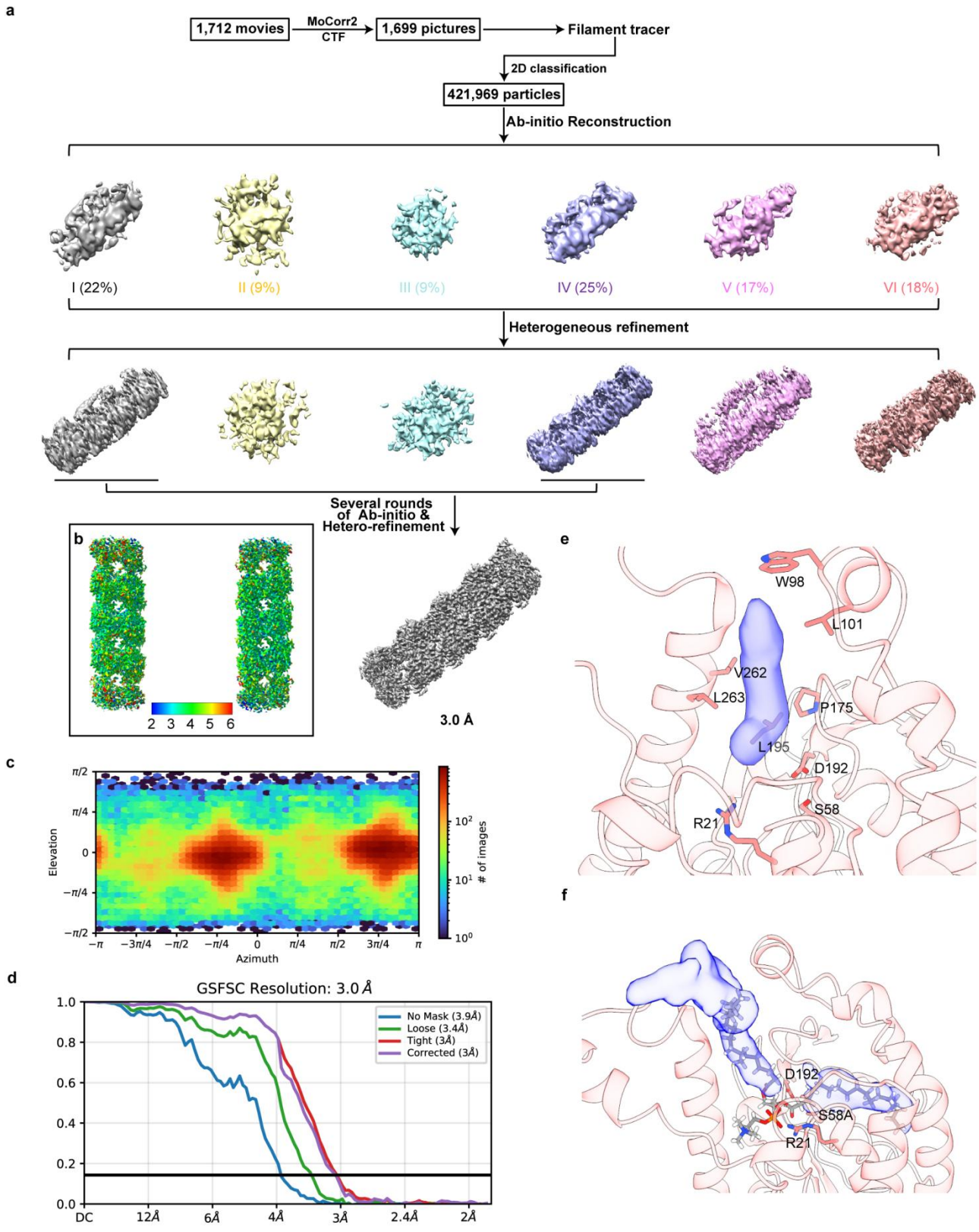

86 **Extended Data Fig. 9 Cryo-EM data processing for *Ab*CapV^{S58A} filament bound**
87 **to 3'3'-cGAMP.**

88 **a,** Flow chart of cryo-EM data analysis of *Ab*CapV^{S58A} filaments. Two
89 homo-oligomers (apo state and intermediate state) were obtained. Reconstructions of

*Ab*CapV^{S58A} filaments **(b)** was coloured by local resolution. The viewing direction distribution plot **(c)** and the 'gold-standard' Fourier shell correlation (FSC) curves **(d)** of *Ab*CapV^{S58A} filaments were presented. **e,** Zoom in on one substrate binding pocket of *Ab*CapV filament with 3'3'-cGAMP bound. Corresponding interactions that contribute to phospholipid binding in *Ab*CapV. **f,** Zoom in on one substrate binding pocket of *Ab*CapV^{S58A} filament with 3'3'-cGAMP bound. Phosphatidylcholine is utilized for modeling. Corresponding interactions that contribute to phospholipid binding in *Ab*CapV.

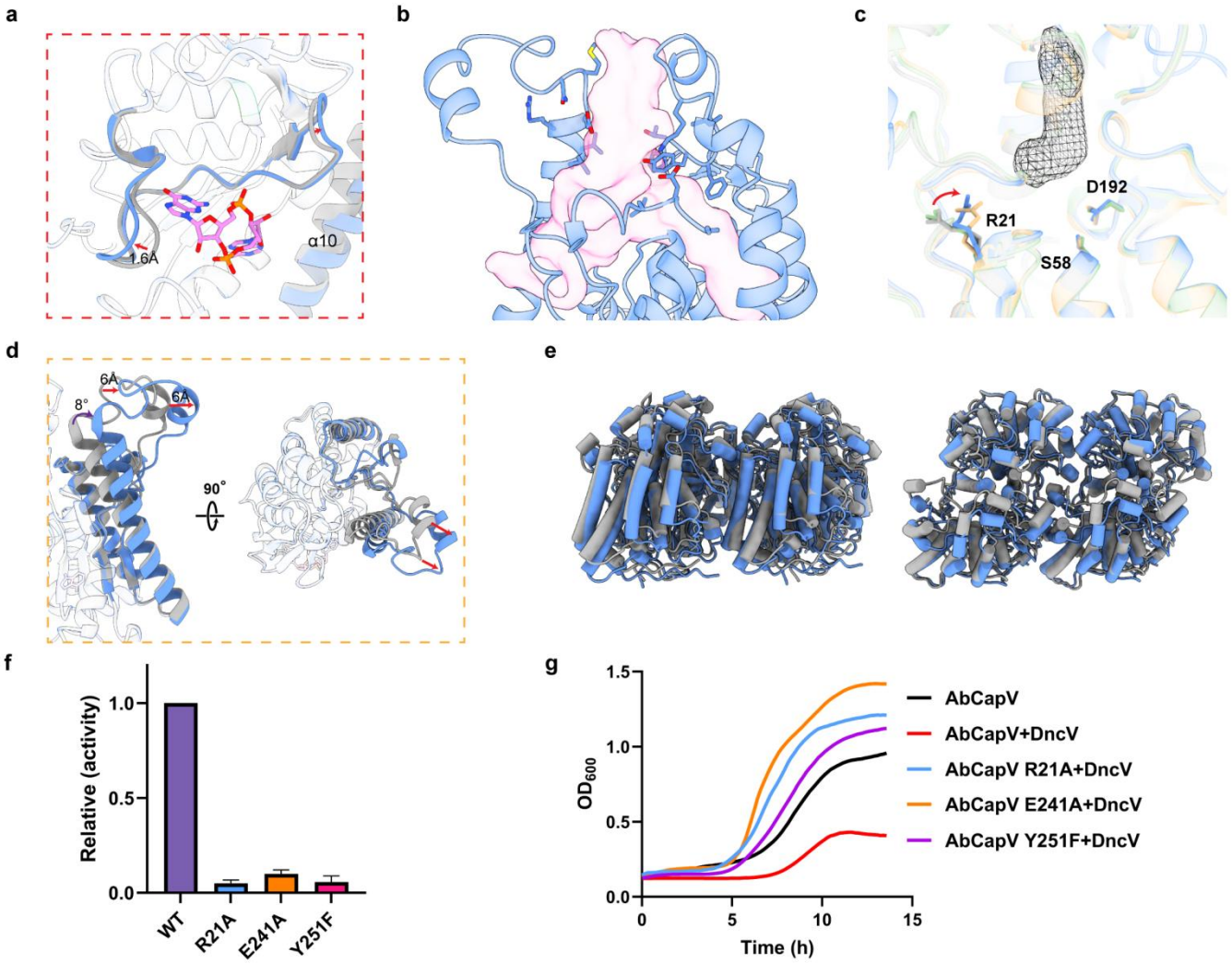

Extended Data Fig. 10 Conformational changes of *Ab*CapV induced by 3'3'-cGAMP.

a, Red box, expanded view of the conformational changes around 3'3'-cGAMP binding pocket. The loop region near residue 156 undergoes a 1.6 Å shift. **b,** Zoom in on one substrate binding pocket of *Ab*CapV filament with 3'3'-cGAMP bound. The conserved phospholipid binding pocket was displayed with red density. **c,** Expanded view of the comparison of R21, S58 and D192. Only R21 showed a significant conformational change. **d,** Yellow box, expanded view of the conformational changes around substrate binding pocket. The arrows indicate the direction of movements after activation. α10 exhibits a pronounced 8° rotation around its C-terminal end, with the starting position of α10 and α9 moving by approximately 6 Å. **e,** Comparison of the tetramer in 3'3'-cGAMP bounded *Ab*CapV filament with the *Ab*CapV tetramer in the apo state. **f,** A bar-graph representation of phospholipid hydrolysis activity measured with the DOPE for a panel of *Ab*CapV R21A, Y251F and E241A. The activity data of the mutants were normalized based on the activity data of the wild-type protein. The error bars indicate the standard deviation for the average of three biological replicates each with three technical replicates. **g,** Growth curves of E. coli expressing *Vc*DncV

and *Ab*CapV wt or R21A, Y251F and E241A. The data are representative of more than three independent biological replicates each with three technical replicates.

Extended Data Video 1 Conformational change of *Ab*CapV from apo tetramer to filament. Chain C (green) has been aligned.

Extended Data Video 2. Procedure of *Ab*CapV activation upon 3'3'-cGAMP binding